Executive summary

Application of CFD for loads predictions over the entire flight envelope

Covered part of flight envelope in this study

CFD at design point

Report no.
NLR-TP-2011-351

Author(s)
J. van Muijden
B.B. Prananta

Report classification
UNCLASSIFIED

Date
March 2012

Knowledge area(s)
Aëro-elasticiteit en vliegtuigbelastingen
Computational Physics en theoretische aërodynamica

Descriptor(s)
aircraft loads
control surfaces
structural flexibility
flow unsteadiness
turbulence model

Problem area

With the objective of achieving a higher efficiency in aircraft design and saving significant development costs, the European aerospace industry has identified the aircraft loads process as a potential candidate for innovations based on state-of-the-art computational methods. Within the current practice of aircraft design, the use of CFD is considered reliable only around the design point. Thus, the aircraft loads process relies heavily on wind tunnel data to obtain the critical aerodynamic design loads of aircraft components over the entire flight envelope. This approach requires the availability of a heavily instrumented wind tunnel model including deflectable control surfaces. The need to manufacture such a model introduces long lead times in the aircraft loads process. As long as the experimental wind tunnel data are not available, engineering estimates for the aerodynamic loads are being used for the initial structural design, leading to a risk of erroneous loads data usage and the potential need to rework the structural design as soon as more accurate loads data become available. A structural design based on high-quality loads data with sufficient accuracy directly at the start of the initial structural design is beneficial in the sense that the

This report is based on a presentation held at the International Forum on Aeroelasticity and Structural Dynamics IFASD-2011, Paris, France, 26-30 June 2011.

structural design can be performed in detail with confidence at a much earlier stage of the design process. Only an a posteriori check of the critical aerodynamic design loads is necessary when the experimental data become available. Due to the improved technology readiness of CFD, it has the potential to fill this gap. However, systematic assessment is needed to increase the reliability for complex flow problems. The work described in this report is intended to support the assessment of the state-of-the-art of Computational Fluid Dynamics (CFD) for sufficiently accurate aerodynamic design loads predictions over the entire flight envelope.

Description of work
Experimental results for the HiReTT configuration with and without deflected ailerons and midboard spoilers, measured at the ETW transonic cryogenic wind tunnel in Cologne, have been used as a test case for the assessment of the current state-of-the-art of CFD for aircraft loads predictions. The selected test cases consist of two different Mach numbers at high Reynolds number, using data obtained with a half span wind tunnel model with deflectable control surfaces. The range of experimental conditions has been computed using fine meshes of 11.8 million grid cells and a two-equation k-ω EARSM turbulence model. The computational and experimental results are compared in terms of overall aerodynamic coefficients, local lift distributions,

pressure distributions, and increments in local lift due to control surface deflections.

Results and conclusions
It is shown that computational results are of high accuracy for attached flow conditions and of acceptable accuracy for separated flow conditions, with an increase in accuracy when wing flexibility is taken into account. Changes in predicted aerodynamic loads due to the deployment of maneuver load alleviation devices are obtained with sufficient accuracy. Comparisons between simulated results and experimental results, however, are found to be distorted to some extent by unwanted semi-span model testing characteristics. For the present small deflections of spoilers and ailerons, the steady CFD-approach is sufficiently robust to achieve converged results over the load factor range of interest, although it can be expected that larger spoiler deflections would necessitate the application of a time-accurate unsteady CFD-approach.

Applicability
The current validation of the ENSOLV flow solver is part of a larger validation effort for CFD-based aerodynamic aircraft loads predictions over the entire flight envelope, using multiple test cases. To date, sufficient confidence has been obtained to apply the flow solver in transonic and supersonic conditions to obtain critical aerodynamic design loads for aircraft structural design.

NLR-TP-2011-351

Application of CFD for loads predictions over the entire flight envelope

J. van Muijden and B.B. Prananta

Approved by:

Author	Reviewer	Managing department
26-04-2012	26/04/2012	26/04/2012

Contents

This page is intentionally left blank.

APPLICATION OF CFD FOR LOADS PREDICTIONS OVER THE ENTIRE FLIGHT ENVELOPE

J. van Muijden[1], and B.B. Prananta[2]

Aerospace Vehicles Division, National Aerospace Laboratory NLR

P.O. Box 90502

1006 BM Amsterdam, The Netherlands

e-mail: [1]muyden@nlr.nl, [2]prant@nlr.nl

Abstract In this paper, the state-of-the-art of Computational Fluid Dynamics (CFD) algorithms to predict aerodynamic loads over the entire flight envelope is determined. Leading European aerospace industries have identified the aircraft loads process as a potential candidate for efficiency improvements by applying CFD-methods in an early stage of the design process to obtain the aerodynamic loads, thereby alleviating the dependency of the loads process on the large lead times introduced by the manufacturing of a detailed and heavily instrumented wind tunnel model. At present, following the continuing developments in computer power, steady Reynolds-averaged Navier-Stokes (RANS) simulations using a two-equation turbulence model are routinely applied, even on very fine meshes, for a vast range of aerospace engineering applications. At the same time, developments in unsteady flow modelling, especially in Large-Eddy Simulation (LES), have matured to the point where the application of hybrid RANS/LES flow models is becoming feasible for demanding applications. The status and limitations of a steady RANS approach in the aircraft loads process are assessed, and prospects of advanced unsteady approaches are discussed.

1 INTRODUCTION

Over the past two decades, significant advances in CFD have led to CFD tools being heavily used in aircraft design studies. One of the remaining challenges for CFD methods is to extend their application in the generation of aerodynamic loads. This will require CFD solutions to be generated at all points of the aircraft maneuver flight envelope [1] and not just close to the design point, see Figure 1. The ability to identify aerodynamic flight loads on aircraft and aircraft components is the key issue in efficient structural component design. An efficient structural component design, meaning that unnecessary weight and volume occupation is avoided as much as possible, is obtained if the occurring loads on the component can be quantified with sufficient accuracy. Consequently, uncertainty margins for structural strength

and deformations can be kept as small as possible, thereby contributing to the main objective of aircraft design, i.e. optimal efficiency.
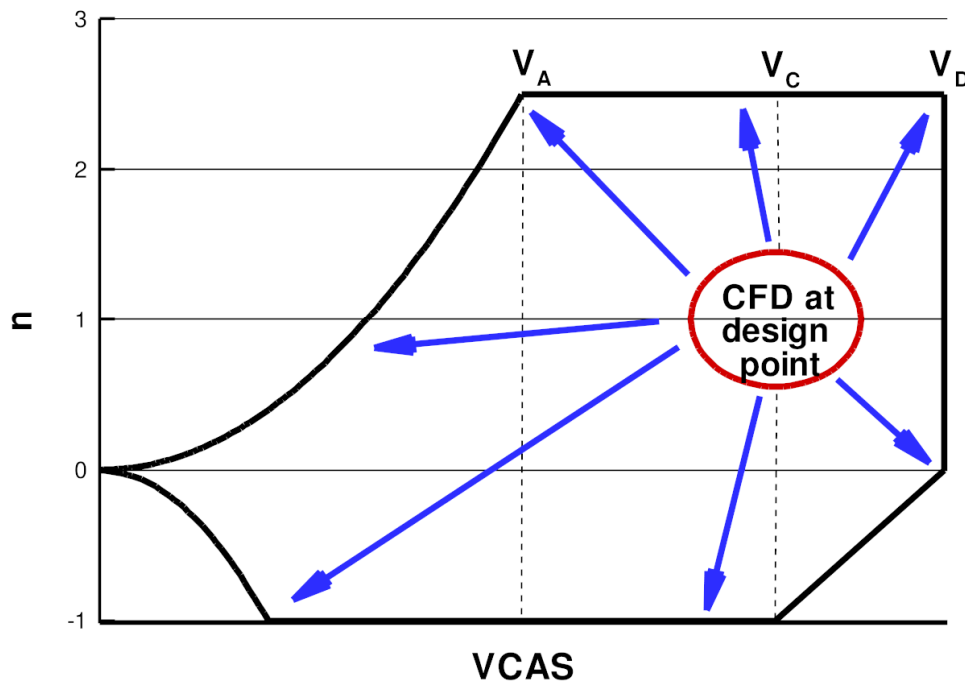

Figure 1: Expansion of CFD capabilities required for use in aircraft loads process

The aerodynamic design loads on the component at hand are derived from the range of loads encountered on the component for each possible flight condition, thus spanning the entire flight envelope. The critical design loads comprise the maximum static loads, supplemented with relevant information on the dynamic content of component loads, and supplemented with information on the number of occurrences of different types of loads. Such information can be gathered experimentally or by predictions.

Currently, within the loads generation process wind tunnel data are used for aerodynamic loads assessment, especially for geometrically complex cases and for off-design conditions. A heavily instrumented wind tunnel model including deflectable control surfaces needs to be manufactured. The need to manufacture a wind tunnel model introduces long lead times into the overall loads process. The model is subsequently tested over a wide range of flow conditions with and without control surface deflections. The advantage of this approach is that, once in the tunnel, the data gathering is very rapid.

The introduction of CFD into the loads process will reduce the lead times associated with the wind tunnel model manufacturing. Instead of using semi-empirical approaches, preliminary aerodynamic loads data can be based on the actual aircraft geometry, thus yielding initial loads estimates of a much higher accuracy. At the same time, the drawback of using CFD is the

significant effort required to generate the loads data for a large number of test conditions. Effective use of CFD leading to an acceptable level of flow solution quality is required involving a thorough understanding of the trade-off between turn-around time and solution quality.

In view of recent developments in CFD-simulations which are linked to the continuing increase in computer power, i.e. the usage of high-density meshes, state-of-the-art turbulence models, unsteady flow modelling, and even more advanced unsteady flow modelling using hybrid RANS/LES methods, the objective of this paper is to assess the state-of-the-art in aerodynamic loads predictions over the flight envelope using a steady CFD approach and to get a clear idea of its limitations as well as prospects for more advanced approaches. For this purpose, aerodynamic loads predictions are compared with experimental results for a semi-span wind tunnel model at high Reynolds number.

2 DESCRIPTION OF TEST CASE

2.1 Test case and experimental data

For the purpose of this paper, the selected test case for loads predictions over the flight envelope is the HiReTT wing-fuselage configuration, although other configurations and tests results are currently subject to further study at NLR. HiReTT is the acronym for the European project "High-Reynolds number Tools and Techniques for Civil Aircraft Design" (active during the years 1999-2002), in which the selected configuration has been developed and tested at the cryogenic European Transonic Wind Tunnel (ETW) in Cologne, Germany [2, 3]. The configuration consists of a fuselage and a wing. Two wind tunnel models have been manufactured and tested, a full-span model on 1/50th scale known as N44 and a semi-span model N47. For a high Reynolds numbers and detailed flow measurements including deflected control surfaces, the current selection of experimental data originates from the 1/30th scale semi-span model N47. The wing of the semi-span model is equipped with a deflectable aileron as well as mountable inboard, mid-span and outboard spoilers. Within the HiReTT-project, testing has been performed for the clean configuration (i.e. without any deflected control surfaces) and for a varying range of deflected control surfaces. The spoilers and ailerons have also been tested in a so-called maneuver load alleviation (mla) setting having limited upward deflections of 10 degrees of both the aileron and the mid-span spoiler to reduce the loads on the outer part of the wing. For the current loads predictions study, the clean as well as the mla-configuration have been selected. Test conditions are available for the range of Mach numbers between 0.2 and 0.96, with Reynolds number variations controlled by fluid pressure and temperature adjustments in ETW. The data selection for the present paper is limited to Mach numbers of 0.85 and 0.93 at

a Reynolds number of 54.1 million. The half-span model in ETW, as well as a close-up of deflected control surfaces for the mla-configuration, is shown in Figure 2.

Figure 2: HiReTT N47 semi-span model in the ETW test section (top), and detailed view of outer wing of mla-configuration with upwards deflected mid-board spoiler and aileron (bottom)

The data of the wind tunnel semi-span model N47 comprises pressure distributions at 7 rows on the wing having 35 pressure orifices each, force and moment coefficients, and local lift coefficients. The location of the pressure sections, aileron and mid-board spoiler are shown in Figure 3.
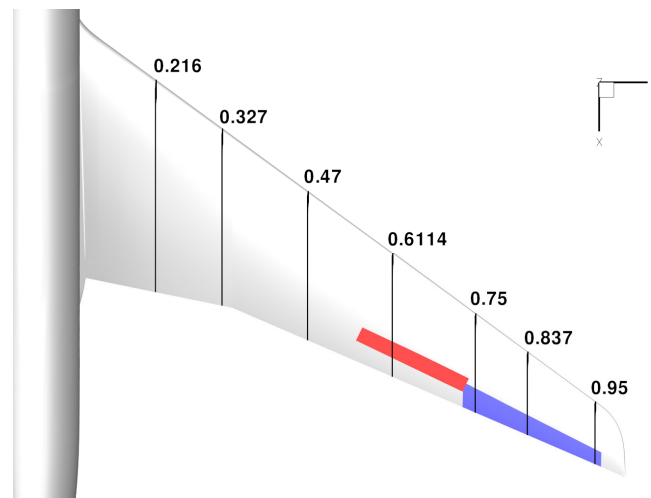
Figure 3: Pressure sections in relation to the location of deflected mid-board spoiler (in red) and aileron (in blue) for the mla-configuration

In this paper, experimental results from semi-span model testing are used for comparison with simulations. Results from semi-span model testing are subject to different wind tunnel wall/ support interferences than those from full-span model testing [4–7]. In this respect, comparisons of simulated results with experimental results from semi-span model testing should be interpreted with care in terms of absolute levels of overall aerodynamic coefficients due to the differences in boundary conditions in the symmetry plane. Comparisons based on increments, e.g. due to deflected mla-devices, are an alternative way to use data from semi-span model testing, although such a comparison is not always feasible.

2.2 Geometry handling and meshing

Two configurations have been selected for the loads predictions study, viz. the clean and the mla-configuration. Since these configurations either have no or rather limited control surface deflections, it has been decided that for both configurations a largely similar continuous computational mesh is still possible with minor adjustments to the actual defining outer mold shape. Following this observation, the outer mold shape of the mla-configuration is slightly adjusted to allow for a continuous shape of the deflected aileron using an S-shaped transition at the sides of the aileron, and the deflected mid-board spoiler is similarly modelled at its sides while at its trailing edge it is modelled as a discontinuous ramp. In this way, the existing gap between spoiler and wing is not included in the CFD-mesh. The resulting surface shape for the mla-configuration as included in the mesh is shown in Figure 4. An alternative meshing approach, making use of discontinuous meshes at block interfaces, has been considered in order to obtain a more detailed deflected spoiler including the gap between spoiler and wing, but such a mesh has not yet been realized. For larger spoiler deflections, such a meshing approach will eventually be necessary.
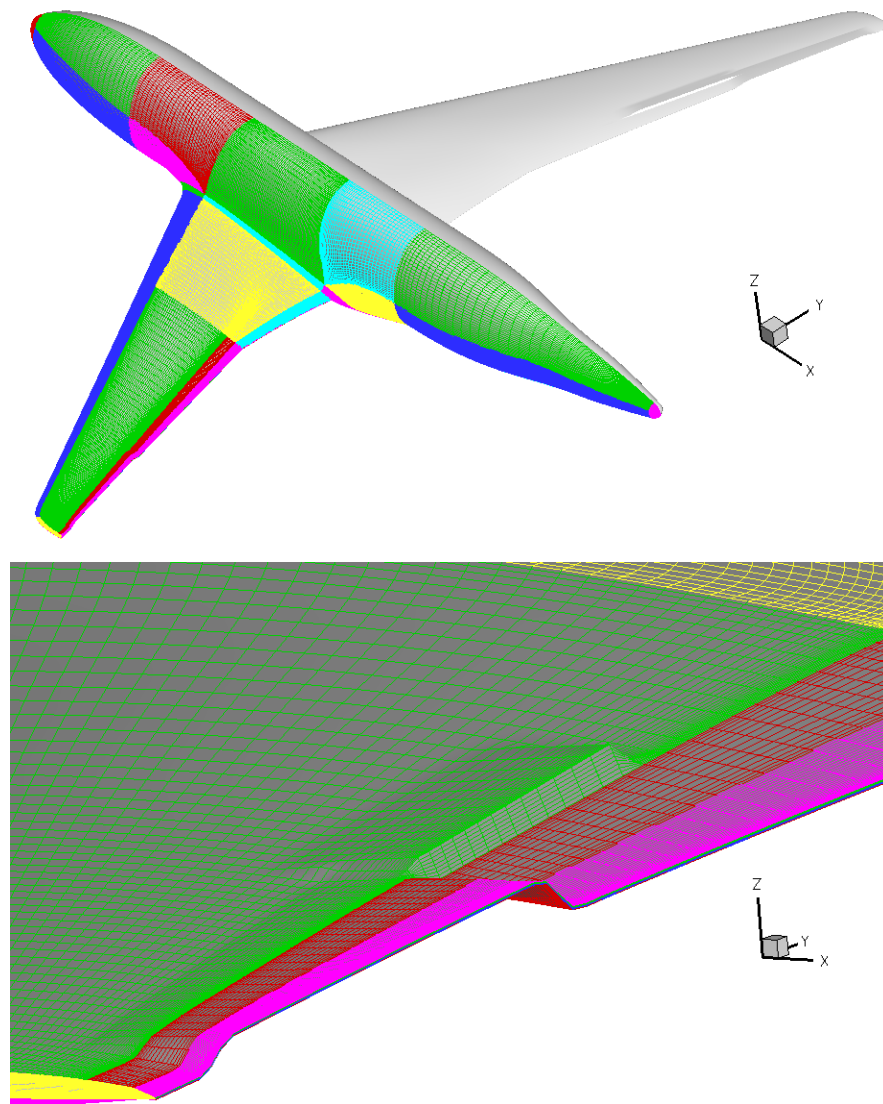
Figure 4: Geometry and final fine surface mesh for the mla-configuration (top), and detailed view of surface mesh near deflected spoiler and aileron (bottom)

Initially, an existing multi-block structured topology and mesh for the clean configuration was taken as starting point, consisting of 1.8 million volume cells in one half of the configuration (in the computations, symmetry boundary conditions are applied to the symmetry plane). However, some doubts about the impact of mesh density on the influence of turbulence models and thus on grid convergence of flow solutions have led to further refinement of the mesh. The final mesh contains 11.8 million cells in one half of the configuration to allow for a detailed capturing of the deflected aileron and spoiler, and the same resolution was also applied to the clean configuration.

2.3 Analysis method

Flow computations have been performed using the multi-block structured ENFLOW system, using a two-equation k-ω turbulence model [8, 9] enhanced with an Explicit Algebraic Reynolds Stress Model (EARSM, [10]). Boundary layers have been assumed to be fully turbulent. The flexibility of the wind tunnel model is implicitly taken into account during the flow simulations. In this approach, the computed aerodynamic loads drive the update of the surface mesh on the basis of a flexibility matrix that is derived from the structural model of the wind tunnel model. An overview of the structural model, the aerodynamic surface grid and the nodes that are used as support points for defining the flexibility matrix is shown in Figure 5. The volume mesh is subsequently updated based on the displacement of the surface mesh using a volume spline procedure. Embedded grid folding checks triggering local elliptical grid smoothing are applied to repair incidental local volume inversions during mesh updates.
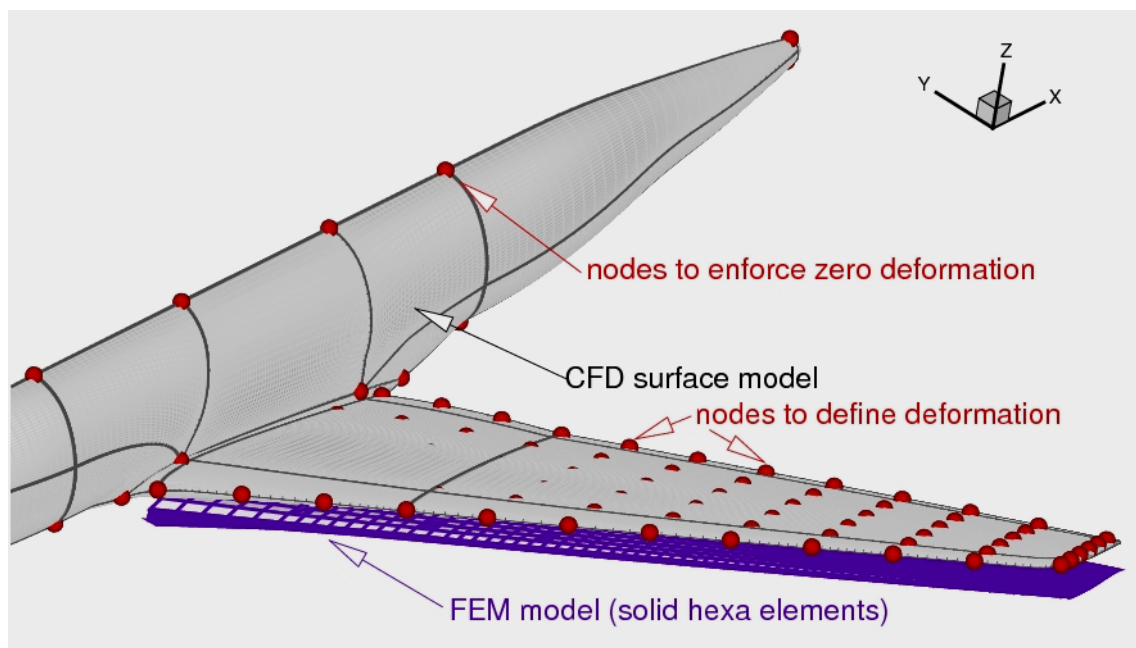

Figure 5: Overview of the structural finite element model and surface CFD grid, showing also the selected nodes used to define the deformation and nodes used to enforce zero deformation at the fuselage

The current high-performance computing environment at NLR is a Silicon Graphics Altix ICE8200 cluster consisting of in total 512 computing cores. This cluster has a peak performance of 5.45 Tflop/s and gives access to 1.5 TB RAM of logically shared memory. The cluster is organized in 64 nodes, each node having 2 quad-core processors. The user is free to claim one or more nodes for a simulation, depending on problem size and preferred turn-around times. Using the fine mesh of 11.8 million cells, a steady Reynolds-averaged Navier-Stokes simulation takes less than 6 hours of turn-around time on a single node. This number indicates that,

overnight, more than one hundred flow conditions can easily be computed. Thus, meshes of more than 10 million cells are no longer a restriction for creating a high number of flow conditions per day, while truly impressive production rates can be achieved on somewhat coarser meshes.

3 AERODYNAMIC LOADS PREDICTIONS

3.1 Aerodynamic loads predictions using steady CFD approach

The common approach for aerodynamic loads predictions is the application of steady-state CFD to obtain flow solutions. At least for conditions with attached flow, this approach is regarded to generate aerodynamic loads within reasonable turn-around times and with acceptable accuracy, depending on appropriately balancing the performance characteristics of available turbulence models and number of mesh points. In the framework of the previously stated objectives, however, the assessment of steady CFD within the aircraft loads process also involves conditions including (partially) separated flow, such as encountered at buffet-onset and stall.

A series of conditions has been calculated for the clean and mla configurations, applying simulations to a rigid as well as a flexible configuration for Mach numbers of 0.85 and 0.93, at a Reynolds number of 54.1 million based on the mean aerodynamic chord. These simulations have been performed for a rigid as well as a flexible wind tunnel model.

3.1.1   Coefficients and pressure comparisons at M=0.85

In Figure 6, the lift curves are depicted for the clean and the mla configuration at a Mach number of 0.85. It is observed that the slope of the lift curve at attached flow conditions is significantly improved by the inclusion of the flexibility of the wind tunnel model. Beyond buffet-onset, however, the differences between predicted values from rigid and flexible simulations are only of minor importance. From buffet-onset up to maximum lift, the predicted lift values are slightly higher than the experimental data, indicating that it is still difficult to get a correct onset of flow separation. Current results as shown in this section are all obtained using the two-equation k-ω turbulence model with EARSM-enhancement, giving predicted values with the highest overall accuracy. Playing around with other available turbulence models (i.e. the TNT k-ω turbulence model [8, 9] in its basic form without EARSM, and an experimental and not yet matured version of an enhanced EARSM-approach) has shown that correctly predicting buffet-onset and stall is highly influenced by turbulence model details in combination with mesh density properties. The margin between missing the onset of flow separation and overly reactions to adverse pressure gradients appears to be small. Nevertheless, from the point

of view of the aircraft loads process, intended for dimensioning of the aircraft structure, it is preferred to be conservative, i.e. having minor overpredictions of loads instead of underpredictions.
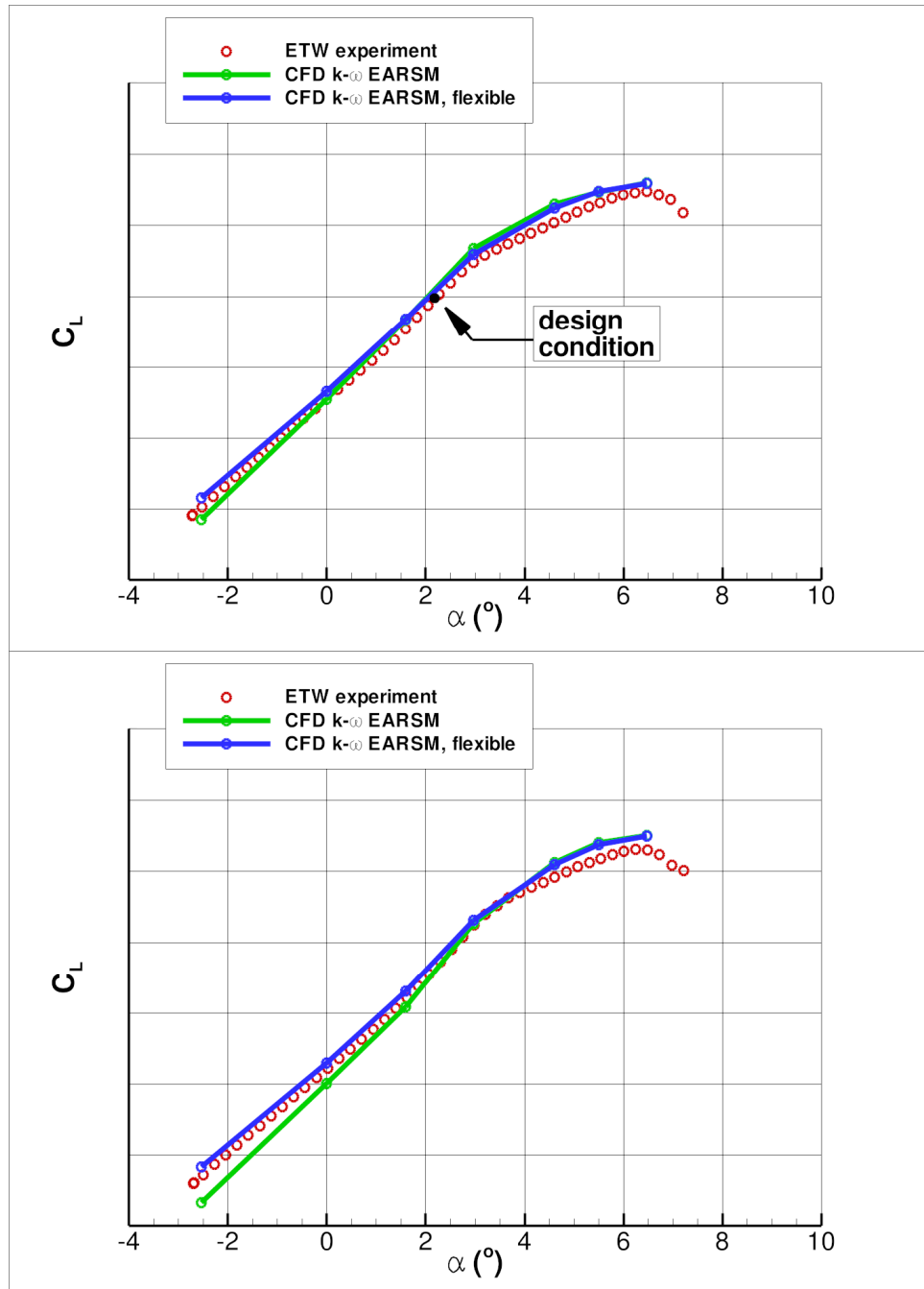

Figure 6: Comparison of lift curves at a Mach number of 0.85 for clean (top) and mla configuration (bottom), rigid and flexible (green and blue lines, respectively). Vertical axis unit equals 0.2.
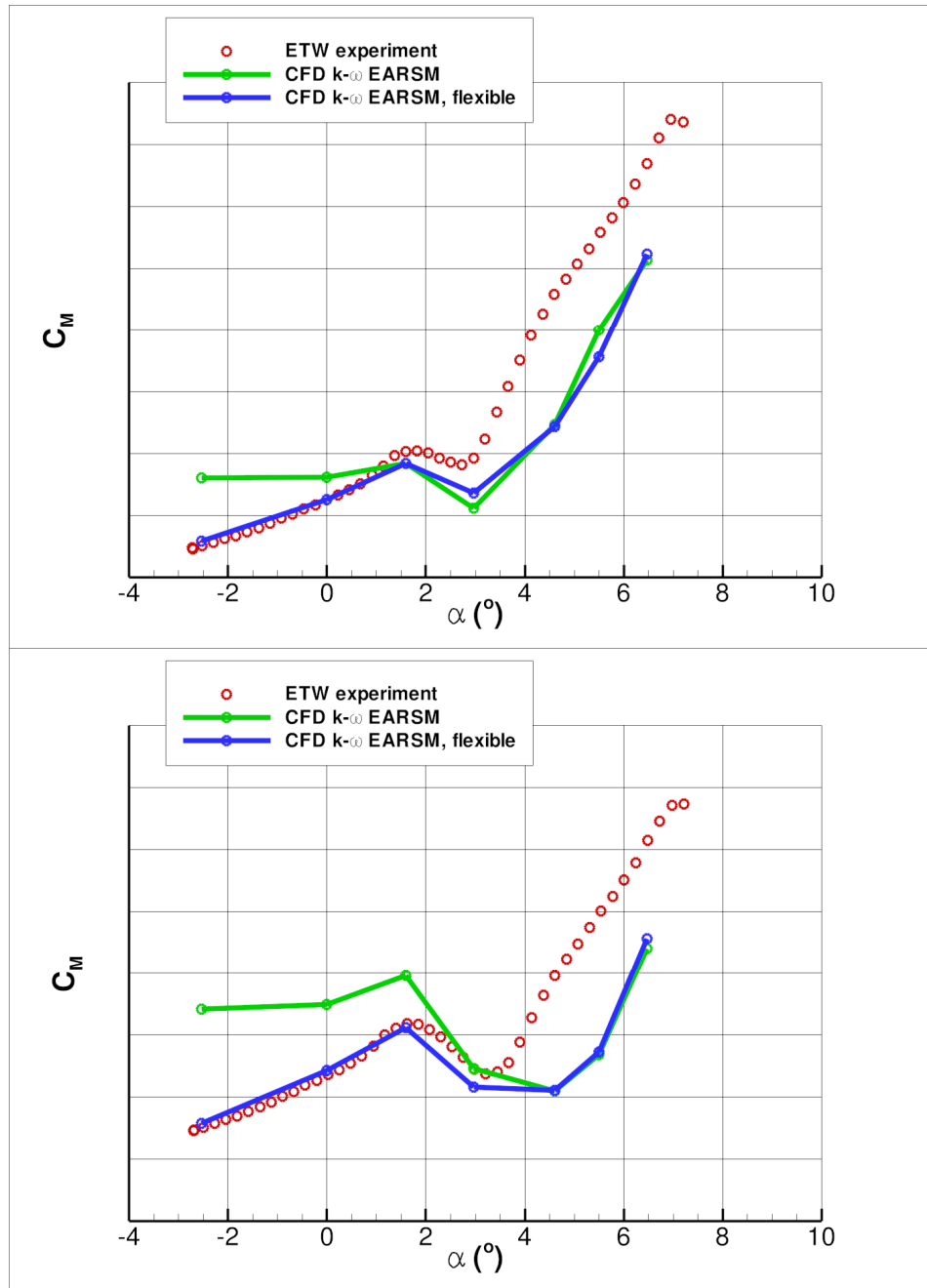
Figure 7: Comparison of pitching moment at Mach number 0.85 for clean (top) and mla configuration (bottom), rigid and flexible (green and blue lines, respectively). Vertical axis unit equals 0.02.

The impact of taking the flexibility of the wind tunnel model into account in the simulations is even more pronounced in the pitching moment behaviour, see Figure 7. At attached flow conditions, the pitching moment coefficients from flexible simulations are significantly better than those from the rigid simulations. The nonlinearity in the curve around buffet-onset is captured by both the rigid and flexible simulations, although with a higher slope accuracy in the

flexible case. Beyond separation-onset, the pitching moment coefficients are smaller than the experimental ones and show no significant differences between rigid or flexible simulations.
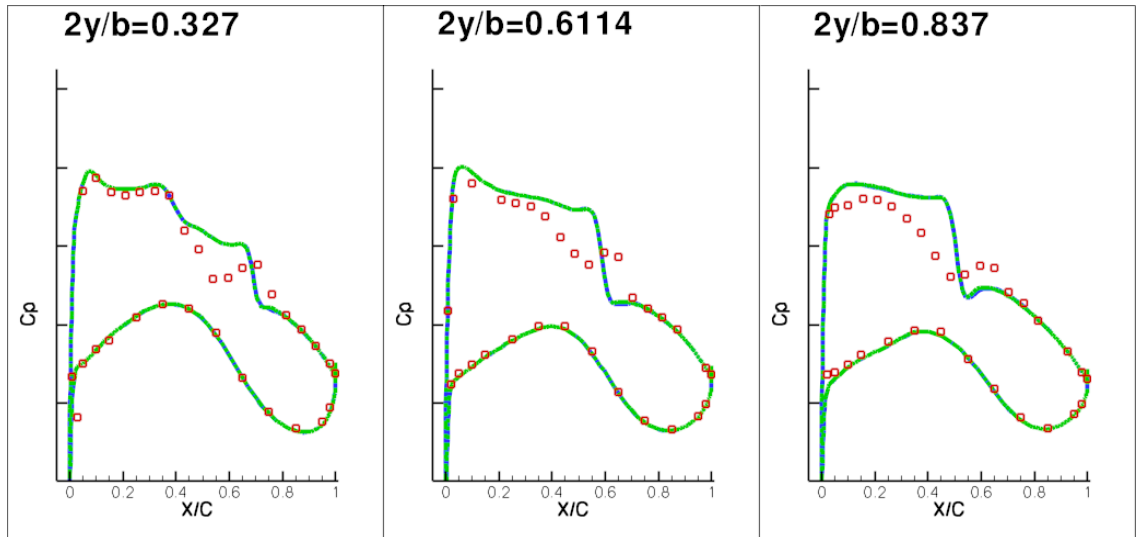

Figure 8: Comparison of pressure distributions on rigid (green lines) and flexible (blue lines) clean configuration, M=0.85, alpha=1.59 degrees, Re=54.1 million. Red dots indicate ETW-experiment. Vertical axis unit equals 0.4.
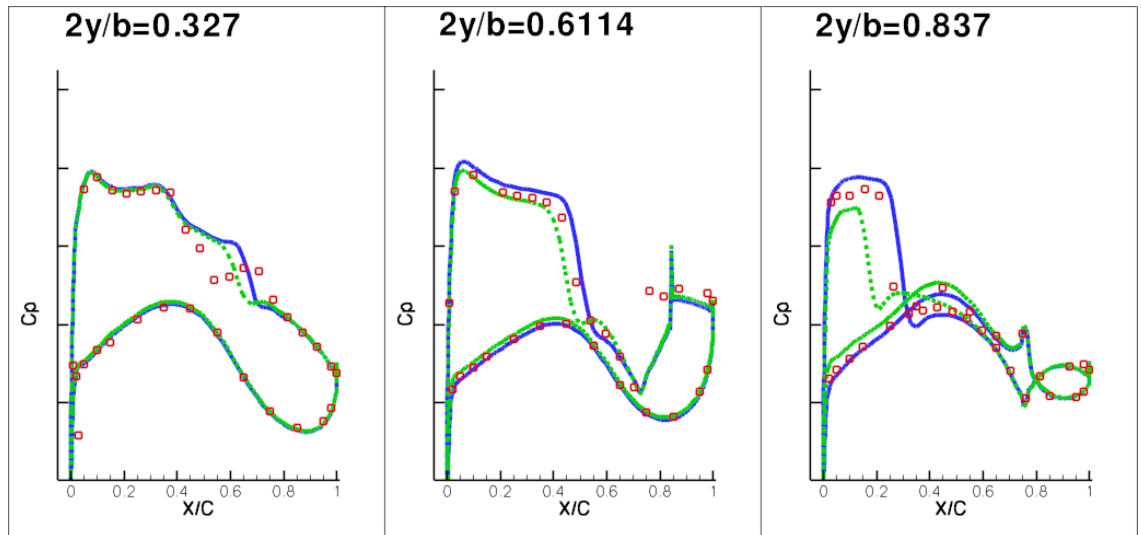

Figure 9: Comparison of pressure distributions on rigid (green lines) and flexible (blue lines) mla configuration, M=0.85, alpha=1.59 degrees, Re=54.1 million. Red dots indicate ETW-experiment. Vertical axis unit equals 0.4.

To support the observations in behaviour of the aerodynamic coefficients, a few comparisons with pressure distributions are shown. In Figures 8 and 9, the results for 1.59 degrees incidence are given. At this condition, the static aeroelastic wing shape of the clean wing is almost identical to the rigid wing shape and therefore the flexible and rigid simulations yield identical

pressure distributions as shown in Figure 8. This finding is reflected in identical aerodynamic coefficients at this condition for the clean wing.

An additional point of attention needs to be mentioned here with respect to the experimental data. There appears to be a double shock system on the inboard wing which is not detected by the simulations. From the comparisons of full-span model and semi-span model test results during the HiReTT-project [3], the appearance of the observed double shock system on the inner wing only occurs on the semi-span model and is most likely related to specific properties of the half model testing process (asymmetric flow, peniche/wind tunnel wall interference). Thus, it should not be expected that the CFD-simulations could have done a better job in this respect.

Following the identical structural characteristics of the wind tunnel model wing (the mla wing only has an added spoiler and a deflected aileron), the rigid wing shape of the mla configuration has not changed and is taken identical to the rigid wing shape of the clean wing. For the mla configuration, the loads on the outer wing are smaller than those on the clean wing due to the deflected devices. The combination of these two factors implies that results of rigid simulations for the mla configuration have a significantly lower local lift on the outer wing than the clean wing. When flexibility is taken into account, the wing shape reacts to the comparatively lower loads on the outer wing by twisting upwards (wash-in), resulting in a higher effective angle-of-attack and consequently higher loads than those of rigid simulations.

The next case is taken at 6.47 degrees incidence, which is close to the maximum lift condition of the experiment. It should be noted that convergence of steady flow solutions is becoming difficult at these conditions due to the development of flow separation. The experimental and simulated results are collated in Figures 10 and 11 for the clean and mla configuration, respectively.

It is observed that results on the inner wing are basically identical for flexible and rigid simulations and are close to the experimental pressure data. However, over the outer wing, the experimental data show separation development from the leading edge onwards which is difficult to predict correctly. As indicated in these figures, at 61 percent span the predictions do not trigger flow separation directly from the leading edge onwards, resulting in locally too much lift. At 84 percent span, the flow separation starting at the leading edge is better captured although the order of rigid and flexible results at that section is somewhat surprising. For the clean wing, see Figure 10, the outer wing flow separation is well captured by the rigid simulation whereas the outer wing loads in the flexible simulation induce wash-out on the outer wing, leading to a partially attached local flow pattern. For the mla wing, as shown in Figure 11, the outer wing loads are comparatively smaller than for the clean wing, leading to less wash-out. As a result, both rigid and flexible simulations show the characteristics of flow separation. Thus,

it is observed that correct predictions at these critical maximum lift conditions are sensitive to the magnitude of wash-out.
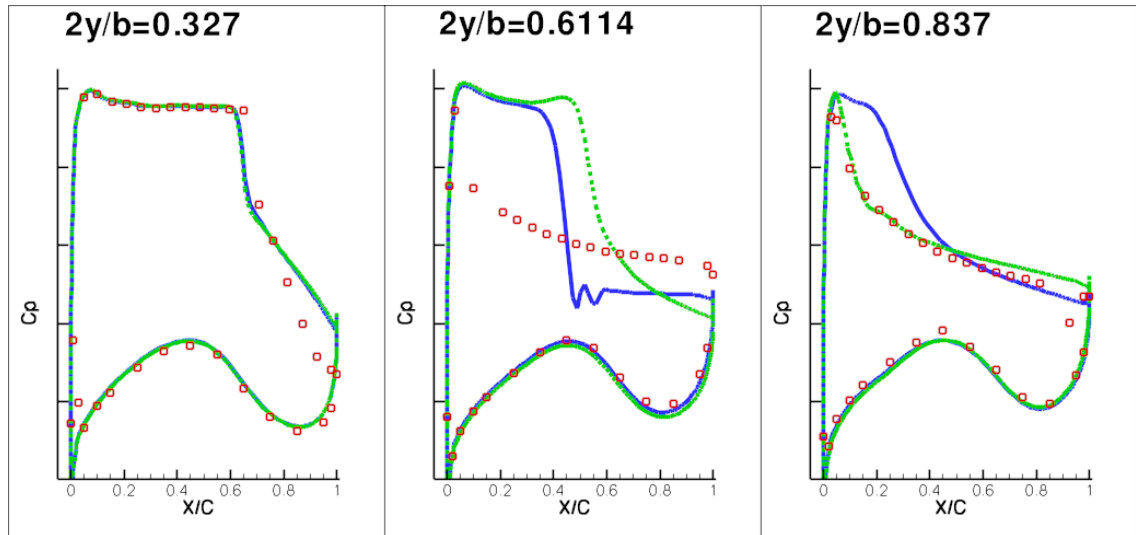

Figure 10: Comparison of pressure distributions on rigid (green lines) and flexible (blue lines) clean configuration, M=0.85, alpha=6.47 degrees, Re=54.1 million. Red dots indicate ETW-experiment. Vertical axis unit equals 0.4.
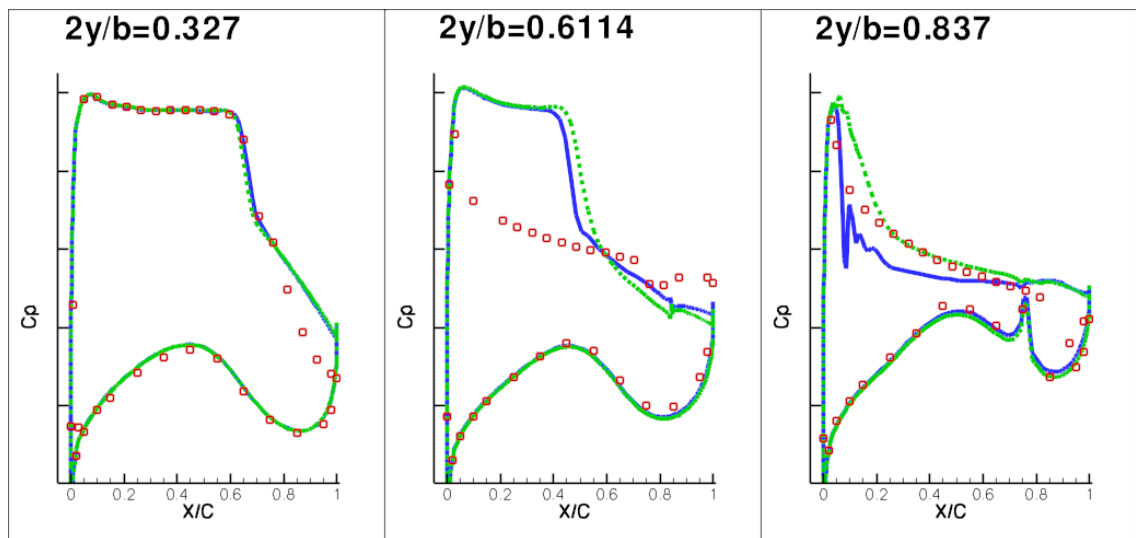

Figure 11: Comparison of pressure distributions on rigid (green lines) and flexible (blue lines) mla configuration, M=0.85, alpha=6.47 degrees, Re=54.1 million. Red dots indicate ETW-experiment. Vertical axis unit equals 0.4.

3.1.2   Coefficients and pressure comparisons at M=0.93

Next, the results at a higher Mach number of 0.93 are scrutinized. For this Mach number, the lift curves are shown in Figure 12. The first striking observation is that the experimental data do not exhibit a maximum lift condition for the range of measured angles-of-attack. The lift continues

17

to increase with incidence. A second observation is related to the difference in lift curves between clean and flexible configurations at lower angles-of-attack. In the experiment, the clean configuration exhibits a mild nonlinearity in the slope around 1 degree incidence which is significantly smaller for the mla configuration. The associated simulated results, either for a rigid or flexible configuration, are shown for the range of conditions for which a steady CFD-result could be obtained. It is remarked that the simulation of results on the basis of steady CFD has not resulted in reliable results for the highest angle-of-attack.
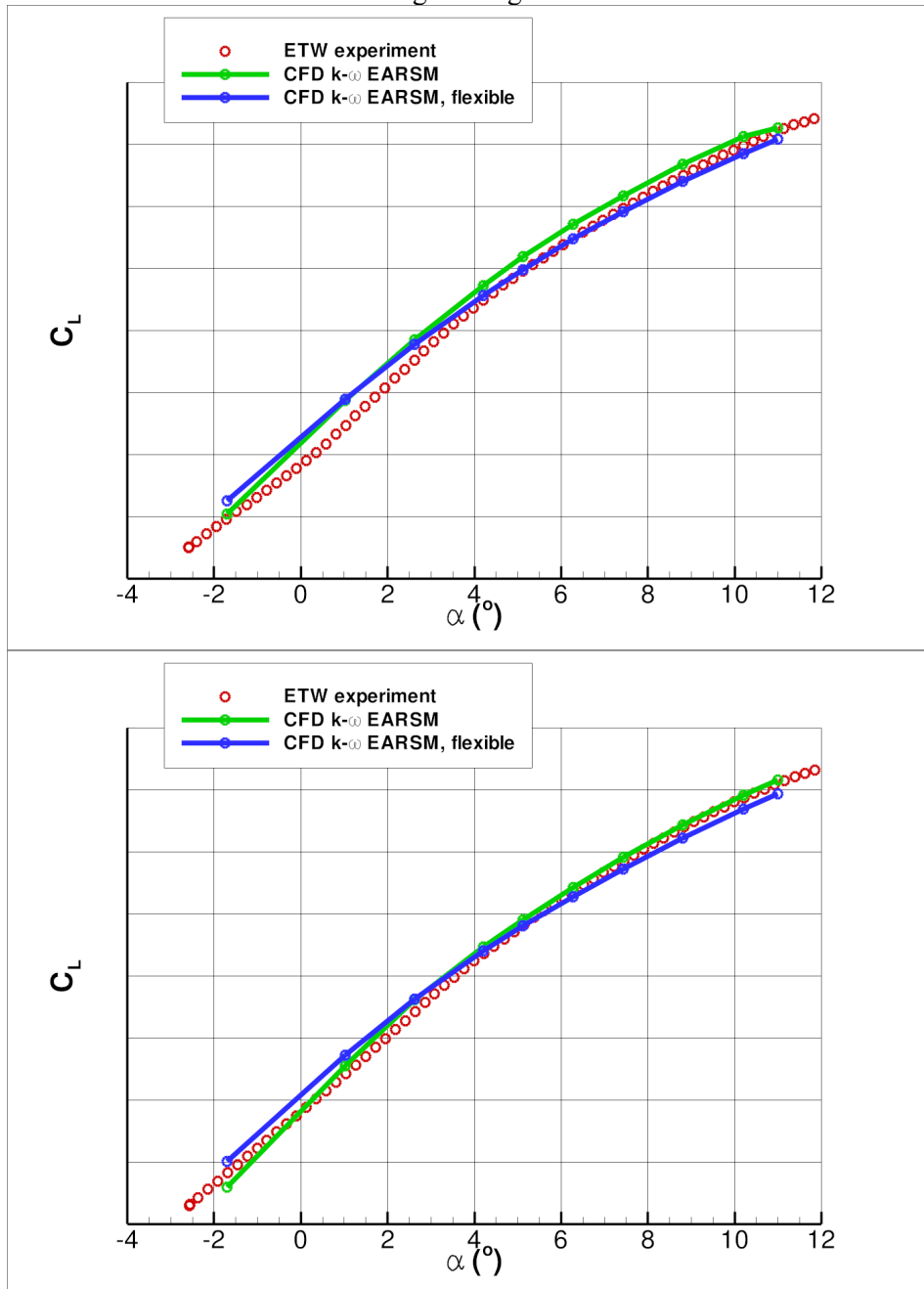

Figure 12: Comparison of lift curves at a Mach number of 0.93 for clean (top) and mla configuration (bottom), rigid and flexible (green and blue lines, respectively). Vertical axis unit equals 0.2.

It is shown in Figure 12 that the rigid simulated results follow the experimental data quite well for incidences in the range of 4 to 11 degrees, both for the clean wing as well as the mla configuration. It will be shown later on that this is a somewhat surprising aspect, since the comparison of pressure distributions indicate that a better comparison with experimental lift coefficients would be expected from the flexible simulations instead. Here, the flexible lift coefficients in the range above 4 degrees incidence are shown to fall a little below the experimental values. For angles-of-attack below 4 degrees, simulated results for the clean configuration show a generally higher lift than the experiment, whereas in the same range of incidences for the mla configuration the rigid results fall on or below the experimental data and the flexible results are slightly above the experimental ones. Generally speaking, the flexible simulations appear to better predict the slope of the lift curve in the lower incidence range, while in the higher incidence range the rigid results appear to better follow the experimental data. This inconsistency will be discussed again when the spanwise loads distributions are compared.

The pitching moment curves are shown in Figure 13. Once again, there is a striking difference in the shape of the experimental curves between the clean and the mla configuration in the lower incidence range, even resulting in an additional change of sign in the slope of the curve for the clean configuration. Simulated results are found to approximately follow the experimental curves when using a rigid wing shape, and the differences with the experiment are reduced when using the flexible wing shape, at least for the higher incidence range. Nevertheless, the slope of the curves is nowhere truly in line with the experimental data, in contrast with the results for the lower Mach number. Here, again, the experimental behaviour for the clean wing at lower incidences is a bit confusing. One would expect that, given reasonable pitching moment predictions for the mla configuration, the same would hold for the clean wing. So, the question remains whether the experimental data at low angle-of-attack for the clean wing are in line with the expectations, and in the following some pressure distributions will be studied to support the understanding of the set of results.

In Figures 14 and 15, a comparison of pressure distributions is given at 2.62 degrees angle-of-attack. At this Mach number, a shock is now also present at the lower side of the wing. The differences between rigid and flexible simulations are small; apparently the wing loading is close to the design loads distribution and the resulting flexible wing shape hardly differs from the rigid shape. It is found that a generally good agreement with experimental pressure data is achieved, except for the rear-loading part at the lower surface. This is rather surprising, since all other cases considered in this paper (and all other computed cases that are not explicitly presented in this paper) show no significant difficulty in predicting the lower surface pressure distribution with high accuracy. Only the cases at high Mach number and lower incidences (angle-of-attack below 4 degrees) appear to display this behaviour.
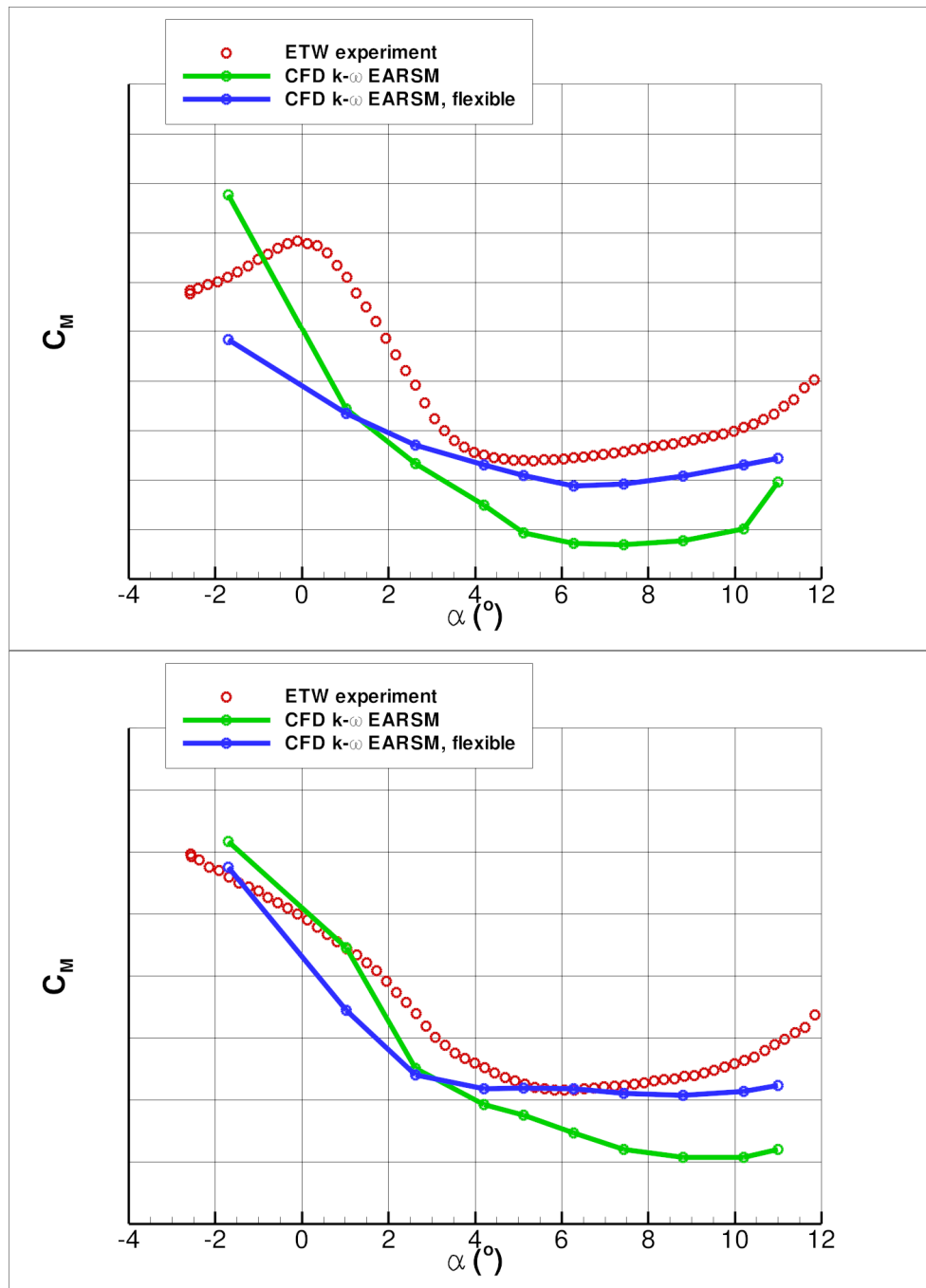
Figure 13: Comparison of pitching moment at Mach number 0.93 for clean (top) and mla configuration (bottom), rigid and flexible (green and blue lines, respectively). Vertical axis unit equals 0.02.
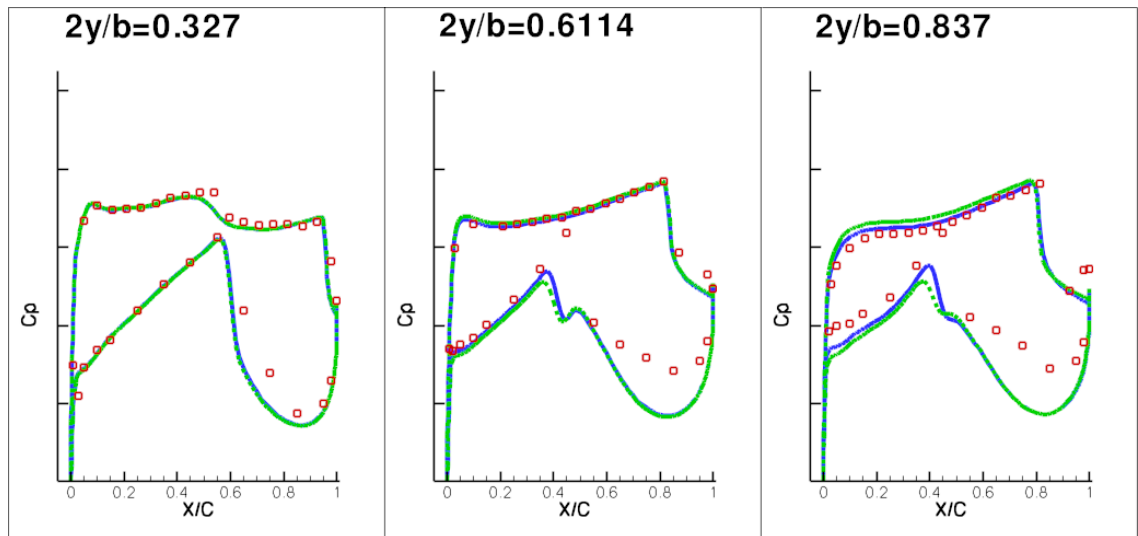
Figure 14: Comparison of pressure distributions on rigid (green lines) and flexible (blue lines) clean configuration, M=0.93, alpha=2.62 degrees, Re=54.1 million. Red dots indicate ETW-experiment. Vertical axis unit equals 0.4.

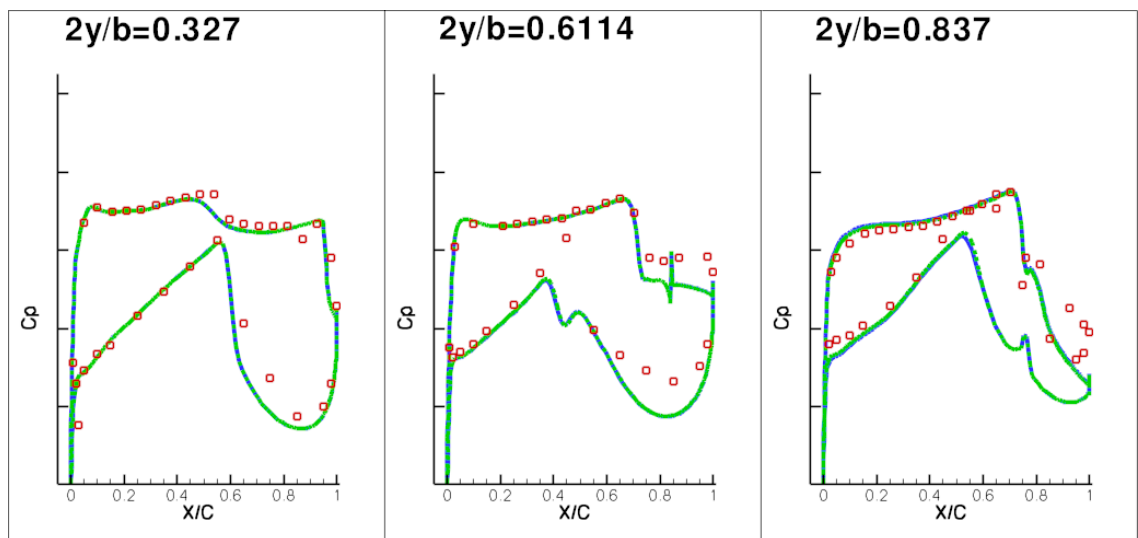Figure 15: Comparison of pressure distributions on rigid (green lines) and flexible (blue lines) mla configuration, M=0.93, alpha=2.62 degrees, Re=54.1 million. Red dots indicate ETW-experiment. Vertical axis unit equals 0.4.

The next case to be considered is at the high end of the lift curves, at 10.2 degrees incidence. The results are shown in Figures 16 and 17. At this condition having a high Mach number and high incidence, almost the full upper side of the wing contains a supersonic region and shock waves are located at or close to the trailing edge. The difference between rigid and flexible results are clear on the outer wing, with flexible data following the experimental pressure data very well, and rigid results showing too high local loads. In view of these observations, it is not consistent that the total lift of the flexible configurations at this incidence is lower than the experimental one when the pressure data exhibit a nearly one-on-one correlation, see Figure 12.
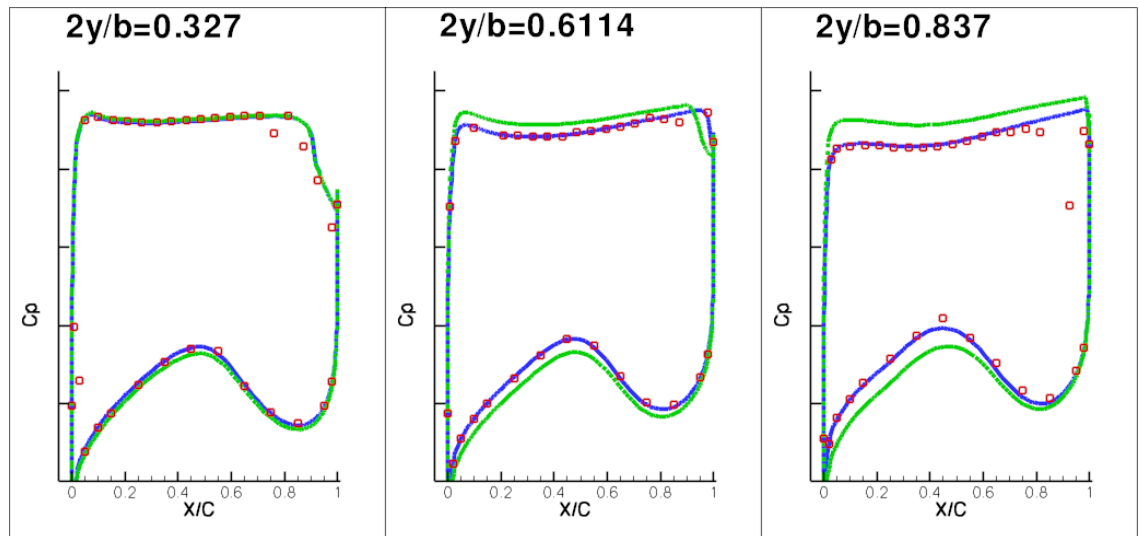
Figure 16: Comparison of pressure distributions on rigid (green lines) and flexible (blue lines) clean configuration, M=0.93, alpha=10.2 degrees, Re=54.1 million. Red dots indicate ETW-experiment. Vertical axis unit equals 0.4.

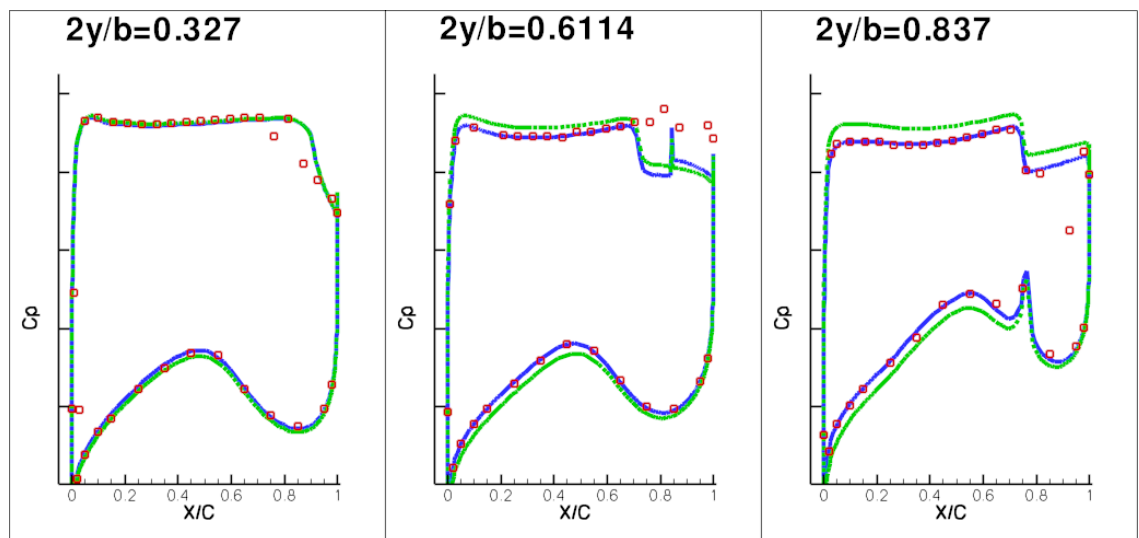Figure 17: Comparison of pressure distributions on rigid (green lines) and flexible (blue lines) mla configuration, M=0.93, alpha=10.2 degrees, Re=54.1 million. Red dots indicate ETW-experiment. Vertical axis unit equals 0.4.

Similarly, the lift coefficient for the rigid configurations is close to the experimental value while the pressure data definitely show more wing loading than needed for this lift value. The pitching moment behaviour in Figure 13 better reflects the expectations based on the wing pressure distributions. It is suspected that peniche/wall interference corrections on the experimental results at high Mach number, correcting the lift contributions of the fuselage, are suboptimal in this case.

3.1.3 Spanwise loads comparisons

A further examination of aerodynamic loads is performed using the spanwise distribution of local lift values. Based on the pressure sections as depicted in Figure 3, the local lift has been determined from the simulated results. Pressure sections from the simulations are obtained by slicing of the surface pressure on the configurations, and the local lift in this way is based on approximately 330 data points per section. Local lift values from the experiment were provided as part of the set of experimental data. Note that the N47 semi-span wind tunnel model is equipped with 7 rows of 35 pressure tappings each.

In Figure 18, the comparison of local lift data is shown for the clean configuration at the two Mach numbers. Each coloured line in this figure corresponds to one of the computed angles-of-attack of which the total lift values are shown in Figures 6 and 12. Only results of flexible simulations are shown here, since the rigid simulations usually give larger local lift values that cannot be compared directly with the experiment. A global impression from the depicted results in Figure 18 is that local lift predictions are acceptable for attached flow conditions, and that the predictions give a slight overprediction of lift on the outer wing. At a Mach number of 0.85, there is a slight increase in deviations between experiment and flexible simulations towards the wing tip. The magnitude of this deviation appears to be rather independent of the angle-of-attack, unless flow separation occurs. At a Mach number of 0.93, this deviation is larger and appears to have a constant value for the higher incidences, while at the lower angles-of-attack the deviation is varying in a more random fashion.

The same data comparison for the mla configuration is given in Figure 19. At a Mach number of 0.85, the correspondence of experiment and simulations are very good for conditions with attached flow. At higher angles-of-attack, the onset of stall is not correctly produced by the simulations which is directly linked to the performance of the turbulence model. The results are in line with the total lift data comparison. At a Mach number of 0.93, it is again found that good spanwise loads predictions are obtained for the higher range of incidences, while larger deviations are observed for the lower set of angles-of-attack. In general, the spanwise wing loads from simulations are larger than the experimental values, contradicting the trend in total lift coefficient at higher incidences where the experimental lift is larger, see Figure 12.
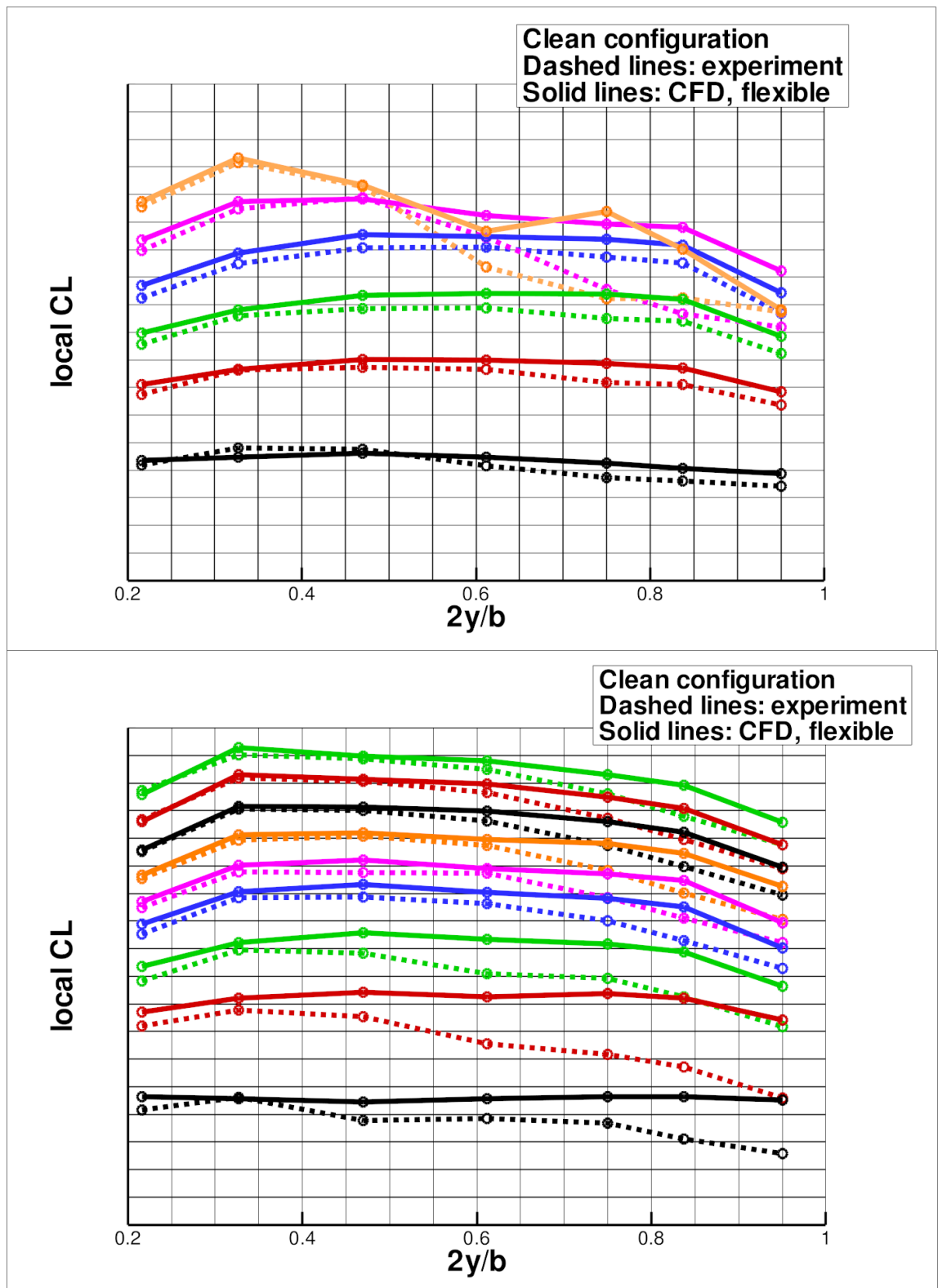
Figure 18: Comparison of spanwise variation in local lift coefficient for clean configuration, M=0.85 (top) and M=0.93 (bottom), Re=54.1 million (vertical axis unit equals 0.1)
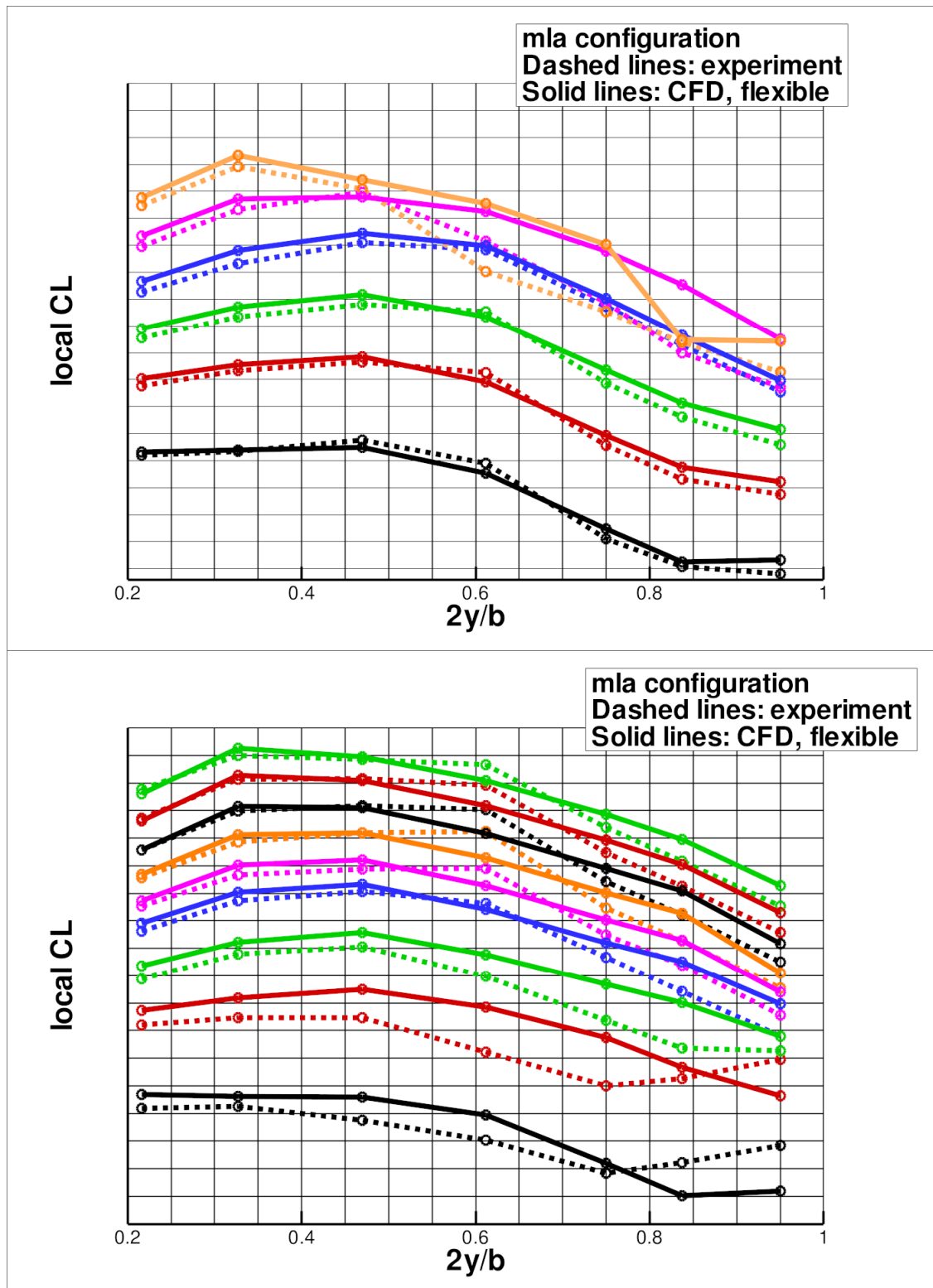
Figure 19: Comparison of spanwise variation in local lift coefficient for mla configuration, M=0.85 (top) and M=0.93 (bottom), Re=54.1 million (vertical axis unit equals 0.1)
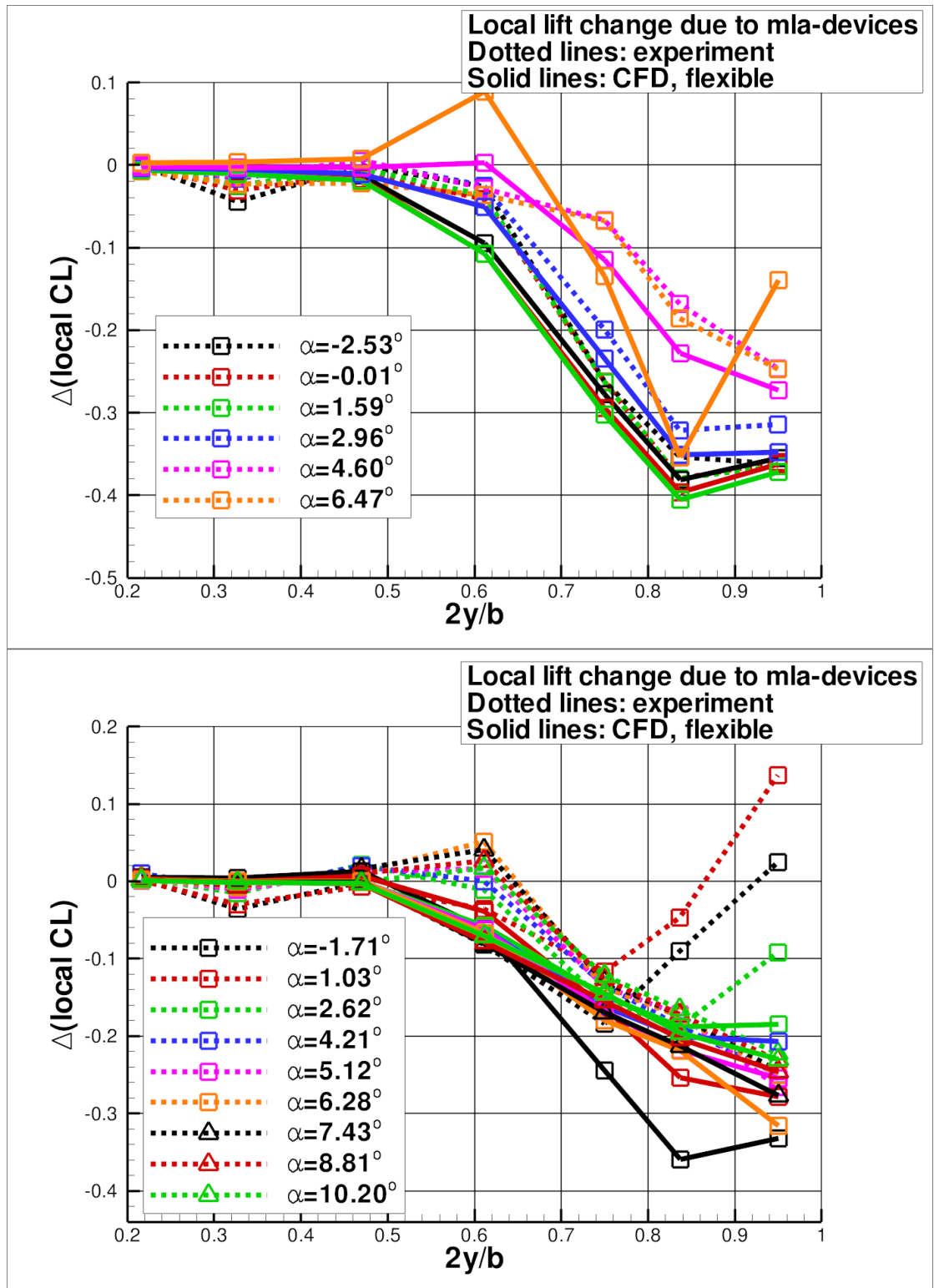
Figure 20: Comparison of spanwise changes in local lift coefficient by deflection of mla-devices, M=0.85 (top) and M=0.93 (bottom), Re=54.1 million

The spanwise loads results are more clearly presented by subtracting the mla configuration lift distribution from the clean configuration lift distribution, showing the changes in local lift along the wing span due to the deflection of the maneuver load alleviation devices. The results are depicted in Figure 20 for both Mach numbers. At a Mach number of 0.85, the local lift reduces with a value of zero at the wing root to about 0.4 at the wing tip. Even though flow predictions at this Mach number are hampered by turbulence modelling issues with respect to stall predictions at large angles-of-attack, the loads increments due to deflected devices are generally well predicted. At a Mach number of 0.93, the local lift reduces from zero at the wing root to a value of about 0.25 at the wing tip, with comparable results from simulations. The outliers here are found at the lowest angles-of-attack, as before, where predictions indicate a larger negative local lift change on the outer wing, whereas the experimental data even indicate a reversal of the expected trend on the outer wing.

3.2 Coverage of flight envelope and limitations encountered

Following the comparison of experimental and simulated results as detailed in the previous section, an impression of the coverage of the flight envelope at the high-end Mach number range using a steady CFD-based loads prediction procedure can now be obtained. In general, simulations using a steady CFD-approach result in loads predictions of acceptable accuracy within reasonably short turn-around times for conditions with attached or mildly separated flow, even on fine computational meshes.

At the cruise Mach number, M=0.85, the loads predictions procedure can be performed until maximum lift which correspondents to a load factor of 1.75, approximately. For these conditions, break-down of the steady CFD-approach is not an issue. However, limitations in physical modelling are encountered in terms of buffet-onset prediction and stall which is directly linked to the applied turbulence model.

For buffet-onset, the initiation of shock-induced separation occurs at the right lift coefficient. The progression of separation, however, does not exactly follow the experimental data and is showing incorrect shock positions and too high loadings. Nevertheless, total lift and resulting spanwise loads are not far off the experimental values and show conservatism in the sense that at least no underprediction is obtained.

For stall predictions, the situation is more complex. By varying the applied turbulence model, it was found that stall predictions are highly sensitive to turbulence model details. Using three different versions of the same two-equation turbulence model, a range of results has been obtained exhibiting stall either too late or too early. The most promising turbulence model in this respect, i.e. the enhanced EARSM version which in its current state leads to premature stall, requires further fine-tuning using data of several test cases to improve the stall prediction.

At the higher Mach number, M=0.93, where no maximum lift is indicated by the experiments, the steady loads predictions procedure can be applied until the steady CFD-approach runs into convergence difficulties. This happens around 11 degrees incidence, i.e. just before the end of the experimental data set which runs until 11.84 degrees. The translation of the condition at a Mach number of 0.93 and 11 degrees incidence to a corresponding load factor yields a value of 3, which is already beyond the normal maneuver envelope limit. Since there are no obvious physical modelling limitations encountered here, curiosity into the break-down of the steady CFD-approach for these demanding conditions has resulted in a time-accurate investigation, which is addressed in the next section.

In conclusion, it appears feasible to cover loads predictions for conditions in the maneuver flight envelope around cruise speeds and beyond by the current steady CFD-approach, provided that the right choice of turbulence model and sufficiently fine computational meshes are selected, see Figure 21. Of course, this conclusion is based on the presented results for one test case only and requires further elaboration for a wider range of Mach numbers and also for other test cases. Nevertheless, the current investigation is one in a row of continuing validation studies relating CFD-simulations to loads and deformations, see e.g. [11-14].
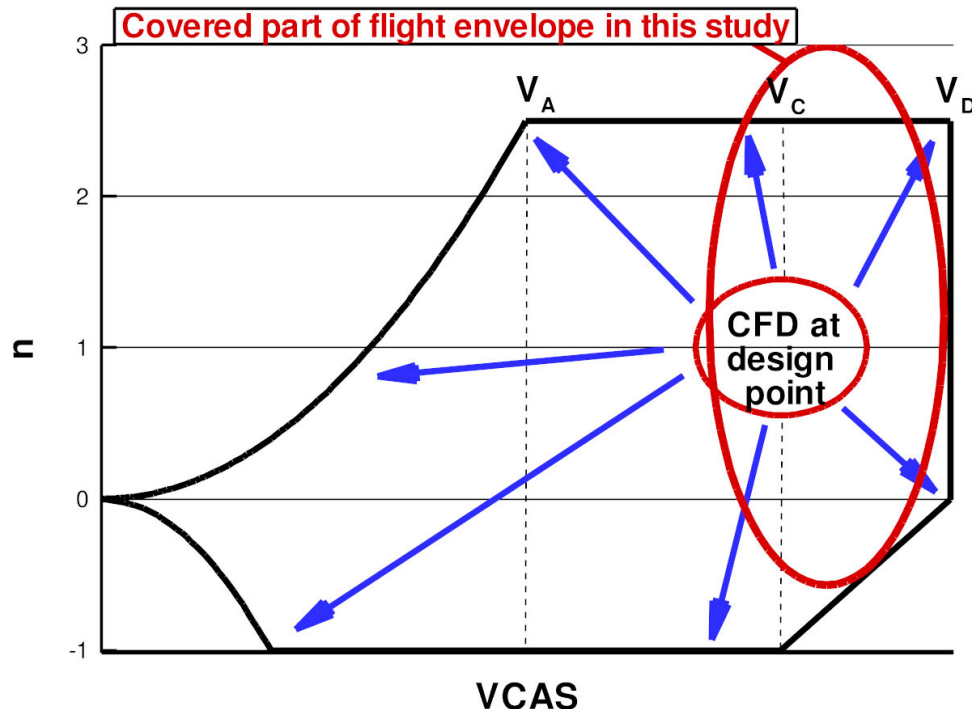

Figure 21: coverage of loads predictions over the flight envelope in the present study, based on the HiReTT test case. Loads predictions for different test cases and different Mach numbers are ongoing.

3.3 Prospects for more advanced approaches

As written in the introduction and as indicated in the previous section, the aircraft loads process is not necessarily limited by the achievements of a steady CFD-approach. Although a steady CFD-approach is desirable for efficiency and productivity reasons in the aircraft loads process, the possibilities of unsteady approaches have increased significantly over the years. Not only has the application of unsteady CFD-based aerodynamic and aeroelastic methods gained momentum, also the emerging higher-order physical modelling in terms of hybrid RANS/LES methods has become an interesting approach for inherently unsteady fluid flow problems. In the following, attention is paid to the computation of conditions that could not be resolved with the steady approach. Some of these conditions exhibit a limitation in the physical modelling, e.g. stall prediction using available turbulence models, while others show numerical convergence difficulties despite the fact that these conditions do not clearly indicate a lack of physical modelling in the applied approach.

The first cases studied in more detail here are the fluid flow conditions both for the clean and mla configuration at a high Mach number of 0.93 and at the maximum experimental angle-of-attack of 11.84 degrees. It has been found that the steady CFD-approach for these conditions results in a stalled residual convergence and oscillatory aerodynamic coefficients. For the purpose of further testing, only rigid simulations have been performed, this time however using a time-accurate unsteady CFD-approach. A typical convergence of aerodynamic coefficients and flow equations residuals is shown in Figure 22. The first number of iterations shows the start-up of the solution process using a steady CFD-approach, starting on a coarse mesh level, continuing on a medium mesh level, and ending on the fine mesh level. Even a restart on the fine level, doing a second set of iterations, does not lead to convergence. The aerodynamic coefficients behave in an oscillatory way, while flow equation residuals are stuck at a high level. Surprisingly, a continuation of the simulation in time-accurate unsteady mode does not reveal any unsteadiness in the flow solution. Instead, the aerodynamic coefficients converge to a steady final state and flow equation residuals decrease several orders of magnitude. Yet, this final steady result requires an unsteady computational approach in order to be obtained.

The final steady results from the unsteady computations have been added to the previously generated results on the basis of a steady CFD-approach, see Figures 23 and 24. The time-accurate results are fully in line with the steady simulation results in the sense that the trends are continued. For the clean configuration, the rigid computations already start to show a reduced slope of the lift curve at 11 degrees, see Figure 22, and this reduced slope is fully in line with the final data point from the unsteady approach. The experimental data, being inherently flexible, do not show this behaviour. Apparently, the reduction of wing twist due to the lifting

29

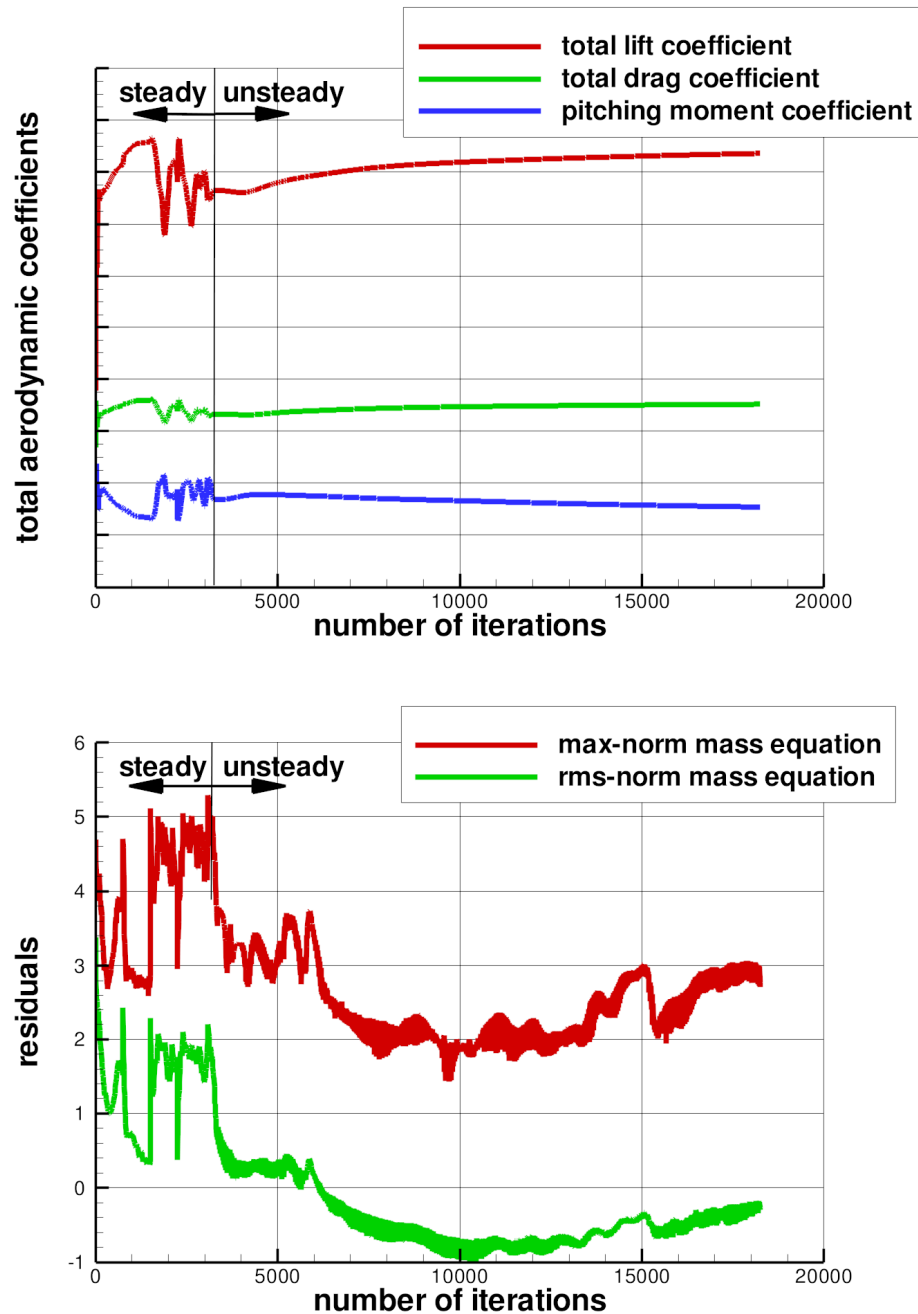loads is just sufficiently large to avoid a noticeable reduction in lift curve slope due to flow separation.

Figure 22: Example of steady and unsteady coefficient convergence (top) and residual convergence (bottom) for a rigid computation at M=0.93, α=11.84 degrees of the mla configuration
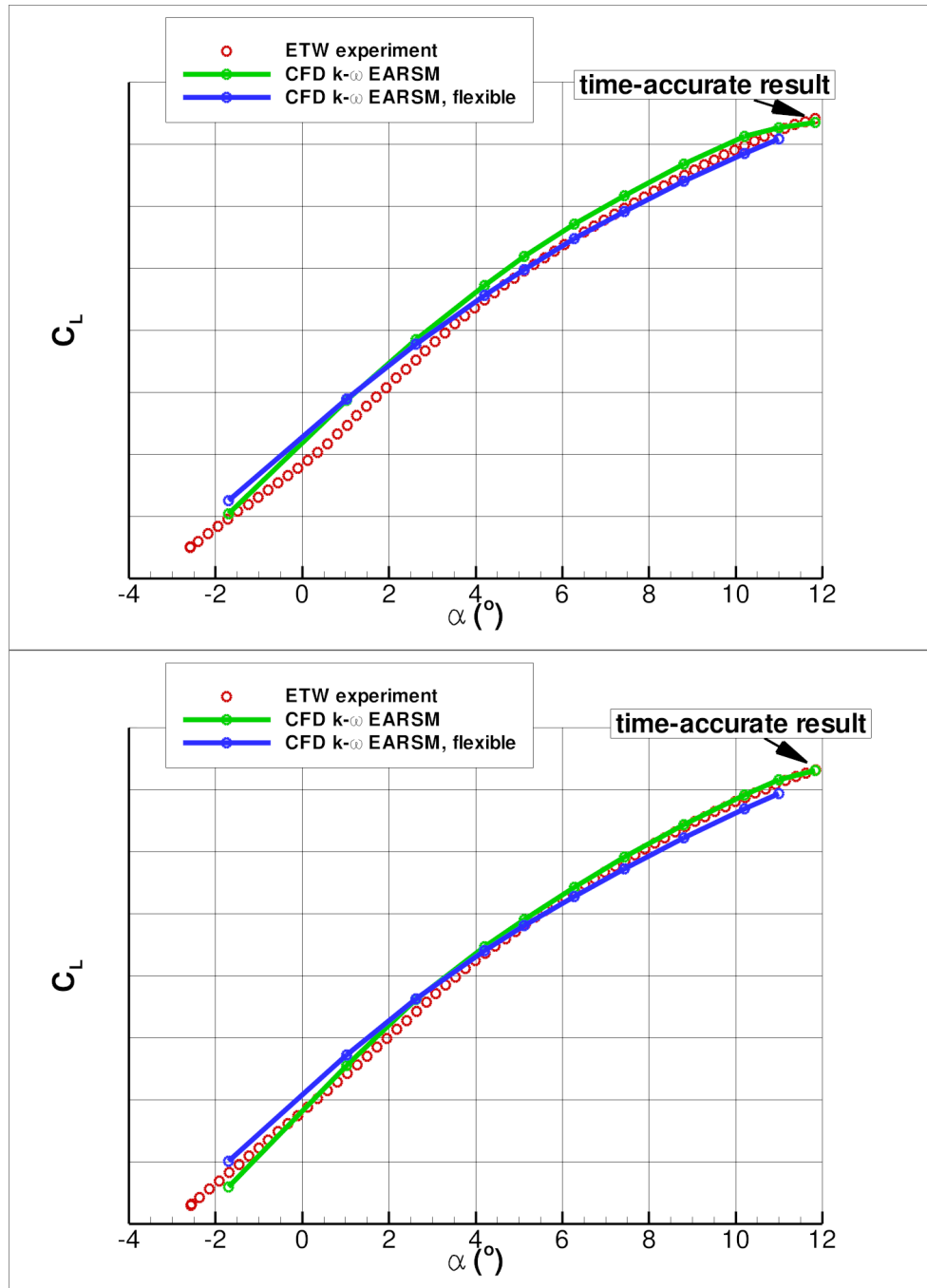
Figure 23: Comparison of lift curves including time-accurate CFD result at a Mach number of 0.93 for clean configuration (top) and mla configuration (bottom), rigid and flexible (green and blue lines, respectively). Vertical axis unit equals 0.2.

The mla configuration, operating at a little bit less lift, manages to keep the existing trend up to the highest incidence. A more sensitive coefficient to examine at maximum incidence is the pitching moment coefficient in Figure 23. Indeed, the experimental data show an increase in slope of the pitching moment coefficient above 10.5 degrees, approximately. Rigid simulations

for both configurations appear to follow this trend, however at a slightly exaggerated rate due to the rigid wing shape assumption.
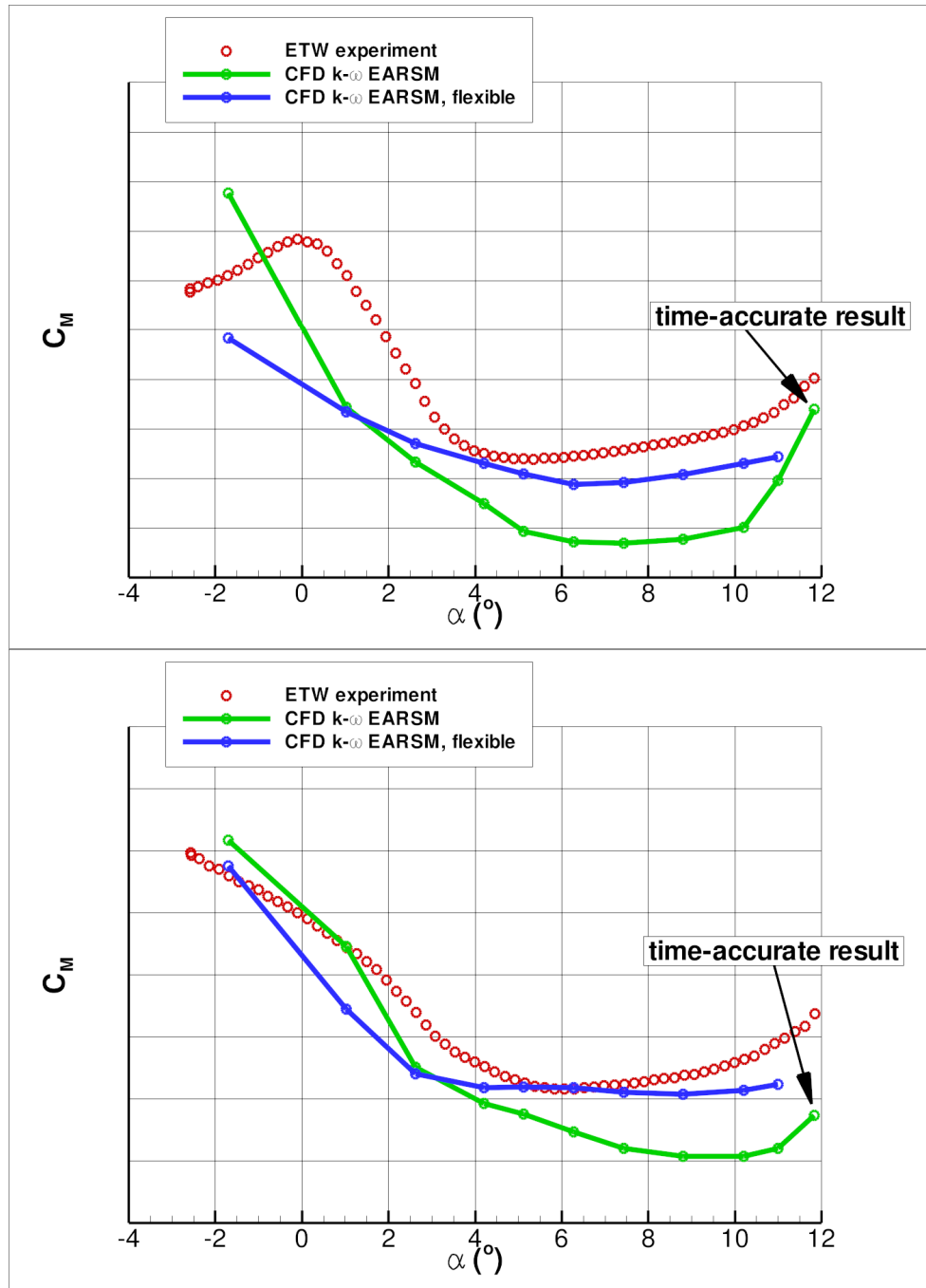

Figure 24: Comparison of pitching moment curves including time-accurate CFD-result at a Mach number of 0.93 for clean configuration (top) and mla configuration (bottom), rigid and flexible (green and blue lines, respectively). Vertical axis unit equals 0.02.

The final remarks in this section concern the computation of unsteady loads beyond stall at a Mach number of 0.85. An attempt to compute loads at incidences higher than 6.5 degrees for the cruise Mach number still resulted in steady flow solutions without the expected drop in total lift, indicating still that a better tuned turbulence model for stall predictions is needed. Also, there was no sign of unsteadiness yet.

An approach that is much more suited to identify unsteadiness in flow solutions around non-moving objects is the hybrid RANS/LES approach [15, 16]. However, even solutions based on this approach depend on the performance of the turbulence model in boundary layers near solid walls, and thus the characteristics of the turbulence model with respect to flow separation determine whether stall is correctly found. At the moment, the only available hybrid RANS/LES approach at NLR is based on the basic TNT k-ω turbulence model. Unfortunately, simulations beyond 6.5 degrees using this hybrid RANS/LES approach only diminish the already developed flow separations. In conclusion, for further simulation studies into unsteady loads predictions it is mandatory to await the advent of a hybrid RANS/LES model based on the k-ω turbulence model with EARSM enhancement.

4 CONCLUSIONS

In this paper, the suitability of applying a steady, multi-block structured CFD approach in the aircraft loads process has been assessed. For this purpose, simulations have been performed for a rigid as well as a flexible configuration with and without deployed maneuver load alleviation devices in the high Mach number range of the flight envelope. Simulated results have been compared with experimental data obtained for a cryogenic semi-span wind tunnel model at high Reynolds number. It has been shown that sufficiently accurate aerodynamic loads predictions can be obtained by simulations for a flexible configuration over a vast range of loads factors up to the edge of the envelope or up to stall, whichever comes first, provided that the steady CFD-approach is based on an appropriate turbulence model in combination with sufficiently fine meshes. Changes in predicted loads due to the deployment of maneuver load alleviation devices are obtained with the correct magnitude. Comparisons between simulated results and experimental results, however, are found to be distorted to some extent by unwanted semi-span model testing characteristics. Limitations encountered in the application of a steady CFD-approach comprise physical limitations of the turbulence model in the correct prediction of stall, and numerical convergence limitations for extremely high-loaded conditions. The latter limitations can be resolved by the application of a time-accurate CFD-approach, while the former limitations requires further development of suitable, generally applicable turbulence models, even for a hybrid RANS/LES approach.

For the currently studied minor deflections of maneuver loads alleviation devices, geometry handling and computational mesh generation have been based on appropriate, minor adjustments to the actual wind tunnel model geometry. The choice for this approach has resulted in the possibility to generate continuous spatial meshes that are as much as possible identical for the clean and the mla configuration. The simulated results showed no noticeable unsteady content. In case larger spoiler deflections need to be modelled, the current meshing approach will eventually not be applicable anymore at which point an alternative meshing approach is envisaged, involving detailed geometrical modelling and discontinuous meshes at block interfaces. Also, larger spoiler deflections are believed to induce inherently unsteady flow fields that could be a fine test case for the assessment of unsteady loads simulations.

5   ACKNOWLEDGEMENTS

6   REFERENCES

[1] Federal Aviation Administration (FAA) - Department of Transportation, Federal aviation regulations part 25 - Airworthiness standards: transport category airplanes, FAR-25, Amdt. 25-23, Washington D.C., 1970.

[2] Elsholz, E., HiReTT – Numerical results vs. wind tunnel tests, paper presented at the European Congress on Computational Methods in Applied Sciences and Engineering (ECCOMAS) 2004, Jyväskylä, Finland, 24-28 July 2004.

[3] Quest, J., Wright, M.C.N., and Rolston, S., Testing of a modern transport aircraft configuration in ETW close to Mach 0.9, paper ICAS 2002-3.8.1 presented at the International Council of the Aeronautical Sciences (ICAS), 8-13 September, 2002.

[4] Boersen, S., and Elsenaar, A., Half-model testing in the NLR high speed wind tunnel HST: its technique and application, AGARD CP 348, 1983.

[5] Gross, N., and Quest, J., The ETW wall interference assessment for full and half models, AIAA paper 2004-0769, 2004.

[6] Gatlin, G.M., and McGhee, R.J., Study of semi-span model testing techniques, AIAA paper 96-2386, 1996.

[7] Doerffer, P., and Szulc, O., High-lift behaviour of half-models at flight Reynolds number, Task Quarterly, Vol. 10, No. 2, pp. 191-206, 2006.

[8] Kok, J.C., and Spekreijse, S.P., Efficient and accurate implementation of the k-ω turbulence model in the NLR multi-block Navier-Stokes system, paper presented at the ECCOMAS 2000 conference, Barcelona, Spain, 11-14 September, 2000, also NLR-TP-2000-144, 2000.

[9] Kok, J.C., Resolving the dependence on free-stream values for the k-ω turbulence model, AIAA Journal, Vol. 38, No. 7, pp. 1292-1295, 2000, also NLR-TP-99295, 1999.

[10]   Wallin, S., and Johansson, A.V., An explicit algebraic Reynolds stress model for incompressible and compressible turbulent flows, Journal of Fluid Mechanics, Vol. 403, pp. 89-132, 2000.

[11]   Prananta, B.B., Meijer, J.J., and Muijden, J. van, Static aeroelastic simulation using CFD - comparison with linear method, paper presented at IFASD-2003, Amsterdam, Netherlands, 4-6 June, 2003, also NLR-TP-2003-530, 2003.

[12]   Prananta, B.B., Namer, A., Maseland, J.E.J., Muijden, J. van, and Spekreijse, S.P., Winglets on large civil aircraft: impact on wing deformation, paper presented at IFASD-2005, Munich, Germany, July 2005, also NLR-TP-2005-366, 2005.

[13]   Muijden, J. van, Improvement and verification of low-speed aerodynamic characteristics of a supersonic civil transport aircraft, Journal of Aerospace Engineering, Vol. 220, No. 6, pp. 569-580, December 2006.

[14]   Laban, M., Soemarwoto, B.I., and Kooi, J.W., Reshaping engine nacelles for testing in wind tunnels with turbofan propulsion simulators, AIAA paper 2005-3703, 2005.

[15]   Kok, J.C., Dol, H.S., Oskam, B., and Ven, H. van der, Extra-large eddy simulation of massively separated flows, AIAA paper 2004-264, 2004.

[16]   Davidson, L., Hybrid LES-RANS: estimating resolution requirements using two-point correlations and spectra, ERCOFTAC Bulletin, Special Issue on "Wall modelling in LES", pp. 19-24, March 2007.